ELSEVIER

Biochimica et Biophysica Acta 1418 (1999) 117–126

BIOCHIMICA ET BIOPHYSICA ACTA
BBA

Water transport by the bacterial channel α-hemolysin

Stefan Paula [1,*], Mark Akeson, David Deamer

Department of Chemistry and Biochemistry, University of California at Santa Cruz, Santa Cruz, CA 95064, USA

Received 6 November 1998; received in revised form 4 February 1999; accepted 11 February 1999

Abstract

This study is an investigation of the ability of the bacterial channel α-hemolysin to facilitate water permeation across biological membranes. α-Hemolysin channels were incorporated into rabbit erythrocyte ghosts at varying concentrations, and water permeation was induced by mixing the ghosts with hypertonic sucrose solutions. The resulting volume decrease of the ghosts was followed by time-resolved optical absorption at pH 5, 6, and 7. The average single-channel permeability coefficient of α-hemolysin for water ranged between 1.3×10^{-12} cm/s and 1.5×10^{-12} cm/s, depending on pH. The slightly increased single-channel permeability coefficient at lower pH-values was attributed to an increase in the effective pore size. The activation energy of water transport through the channel was low ($E_a = 5.4$ kcal/mol), suggesting that the properties of water inside the α-hemolysin channel resemble those of bulk water. This conclusion was supported by calculations based on macroscopic hydrodynamic laws of laminar water flow. Using the known three-dimensional structure of the channel, the calculations accurately predicted the rate of water flow through the channel. The latter finding also indicated that water permeation data can provide a good estimate of the pore size for large channels.

Keywords: α-Hemolysin; Water channel; Water transport; Biological membrane; Pore size

1. Introduction

The bacterial toxin α-hemolysin secreted by *Staphylococcus aureus* damages cells by forming large pores in the cell membrane [1,2]. The subsequent leakage of molecules and ions from the cell interior leads ultimately to cell disruption. α-Hemolysin, for instance, causes rapid osmotic swelling of erythrocytes, followed by membrane rupture and the release of hemoglobin (hemolysis).

Before the three-dimensional structure of α-hemolysin was solved by X-ray crystallography [3], the pore-forming properties of the channel, particularly its pore size, were commonly explored by marker release studies in small lipid vesicles [4]. In typical experiments aimed at assessing the pore diameter, radioactively labeled molecules of various sizes were enclosed in the vesicles. The cut-off size above which marker molecules did not penetrate the pore was used to estimate its approximate dimensions. Alternatively, the pore size has been predicted from single-channel conductance measurements of α-hemolysin incorporated in planar lipid bilayers [5–7].

* Corresponding author. Fax: +49 (89) 8578-3557; E-mail: paula@biochem.mpg.de

[1] Current address: Department of Membrane Biochemistry, Max-Planck Institute of Biochemistry, Am Klopferspitz 18a, 82152 Martinsried, Germany.

0005-2736/99/$ – see front matter
PII: S0005-2736(99)00031-0

This method has the drawback that the correlation between channel conductance and pore size is not necessarily straightforward [8].

In this study, the ability of α-hemolysin to facilitate water permeation in erythrocyte membranes was investigated by determining single-channel permeability coefficients for osmotically driven water permeation. The dependence of channel activity on pH was also determined. By comparing the experimental results to predictions based on the three-dimensional channel structure [3], it was shown that the single-channel water permeability coefficient correlates well with the pore geometry. Although the measurement of water permeation through channels has typically been carried out in cases where the biological function of the channel is water transport [9,10], the results reported here demonstrate that this approach can also provide valuable structural information on much larger pores such as α-hemolysin.

2. Materials and methods

2.1. Materials

Lyophilized α-hemolysin from *Staphylococcus aureus* was purchased from Calbiochem (La Jolla, CA, USA). Aliquots were hydrated in 10 mM sodium phosphate buffer (2 μg/μl) at pH 7.2 and stored at −25°C. The hemolytic activity of the toxin was assayed according to Bernheimer [11] and was in the range specified by the vendor. Rabbit blood for the preparation of red cell ghosts was collected and stored in glass tubes coated with EDTA. The blood was washed in isotonic buffer composed of 150 mM sodium chloride, 5 mM sodium citrate, and 5 mM HEPES at pH 7.25. After centrifugation at $1000\times g$ for 10 min, the white coat on top of the pellet was removed and the cells were resuspended in a volume of isotonic buffer necessary to give the original volume of the blood sample. Samples prepared by this procedure were stored in the refrigerator until required for experiments. Chemicals were of analytical grade and used without further purification.

2.2. Preparation of erythrocyte ghosts

Red blood cell ghosts were prepared according to the procedure described by Steck and Kant [12]. Several ml of washed blood cells were diluted into 25 volumes of chilled buffer composed of 4 mM potassium sulfate, 0.2 mM sodium citrate, and 0.2 mM HEPES (buffer A) at pH 7.0. The mixture was stirred on ice for 5 min and then centrifuged at $12\,000\times g$ for 8 min. The pellet was washed once more in buffer A, followed by two additional washing cycles in a buffer made from 100 mM potassium sulfate, 5 mM sodium citrate, and 5 mM HEPES (buffer B) at pH 7.0. Throughout the washing cycles, the sample was always kept on ice or in a chilled centrifuge. The pellet of the last centrifugation step was diluted into a volume of buffer B that was required to obtain the original volume of the blood sample. The ghosts were sealed by incubation at 37°C for 1 h.

2.3. Measurement of water permeation in unmodified ghosts

Osmotically induced water permeation was measured by monitoring the kinetics of volume changes of ghosts upon dilution into hypertonic solutions [9,13–15]. This method relies on the linear relationship between the volume of the ghosts and the reciprocal of the optical absorbance of the sample. It is furthermore necessary that the ghosts behave as ideal osmometers, meaning that their real volume matches the volume expected from the concentration of the osmotically active solute. This condition is also known as the 'Boyle-van't Hoff law' [15]. To test the validity of this relationship, 200 μl ghosts were mixed with 2 ml buffer B which contained various concentrations of the membrane-impermeable solute sucrose (0, 50, 100, 150, and 200 mM). After equilibration (15 min), the absorbance spectrum of each sample was recorded between 300 nm and 750 nm. The ratio of the ghost volume after and before shrinkage, V_{eq}/V_i, was calculated from the internal solute concentration before (c_i) and after shrinkage (c_{eq}):

$$\frac{V_{eq}}{V_i}=\frac{c_i}{c_{eq}}=\frac{c_i}{c_i+\Delta c}. \quad (1)$$

Here, c_i is the concentration of all the solutes in buffer B and Δc is the concentration of sucrose present in the external medium.

In order to determine the water permeability coefficients of the ghosts, the time-dependence of the optical absorption at 350 nm was monitored. In a typical time-resolved experiment, a small aliquot (150 or 300 μl) of ghosts was mixed with 2 ml hypertonic buffer in a stirred cuvette. The hypertonic buffer contained 100 mM sucrose, glucose or polyethylene glycol (average molecular weight: 400 g/mol) in buffer B. The resulting volume decrease of the ghosts was followed for 300 s by recording the optical absorbance at a wavelength of 350 nm with a Hewlett-Packard 8452 spectrophotometer (Palo Alto, CA, USA).

2.4. Measurement of water permeation through α-hemolysin

To study the effect of α-hemolysin on water permeation, ghosts were treated with varying amounts of the toxin. The concentrations of α-hemolysin were adjusted to yield a nominal channel to ghost ratio of 100, 200, and 1000. To achieve maximum insertion of toxin into the ghost membranes, the samples were incubated at 37°C at pH 7 for 1 h and then maintained at room temperature for an additional 12 h. Before use, the samples were centrifuged at $12\,000 \times g$ for 8 min and washed twice with buffer B. To assess the amount of free α-hemolysin after incubation, the supernatant of the first centrifugation step was assayed for hemolytic activity [11].

Water permeability measurements were carried out as described above using exclusively 100 mM sucrose in buffer B as the hypertonic solution. To investigate the effect of pH on toxin-induced water permeation, the ghost suspensions prepared at pH 7 were titrated to lower pH-values (pH 6 and 5) with small amounts of sulfuric acid. After a waiting period of at least 10 min, water permeation experiments were performed by mixing ghosts (150 μl) with 2 ml 100 mM sucrose solutions prepared in buffer B. The pH of the hypertonic buffer was identical to the pH of the ghost sample. Unless indicated otherwise, all experiments were carried out at room temperature.

For the determination of the activation energy of channel-mediated water transport, permeability measurements were performed at 10, 20, 30, and 40°C. The temperature of the samples was kept at the desired level with the aid of a circulating water bath connected to the cuvette holder of the spectrophotometer. Samples used in the temperature-dependent measurements had a pH of 7 and a channel to ghost ratio of 200.

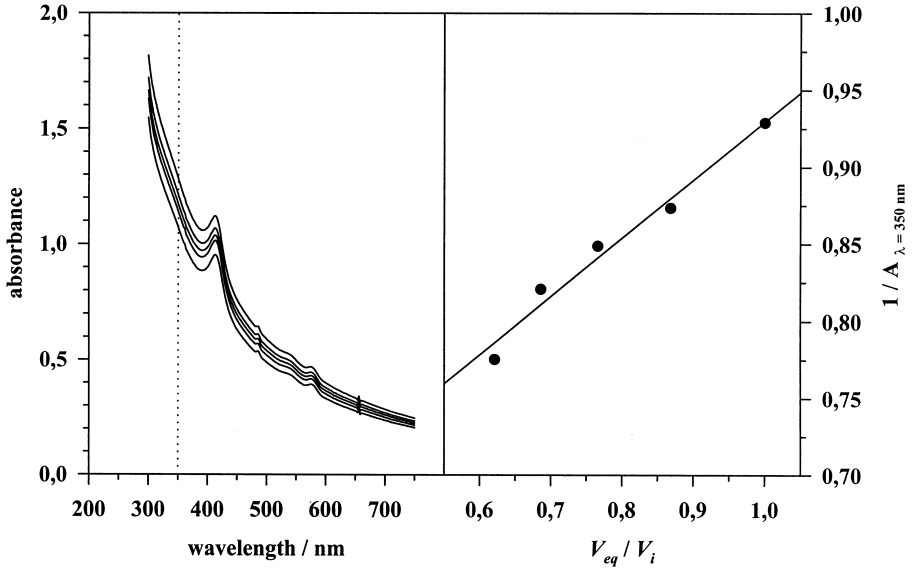

Fig. 1. Relationship between optical absorbance and relative volume of ghosts. Left panel: Spectra of ghost samples after equilibration in hypertonic sucrose solutions (0, 50, 100, 150, and 200 mM). The uppermost spectrum corresponds to 200 mM sucrose and the lowest spectrum to 0 mM sucrose. Right panel: Reciprocal of absorbance at 350 nm versus calculated ghost volume at equilibrium (V_{eq}) divided by the initial volume (V_i). The line was calculated by linear regression and confirms the validity of the Boyle-van't Hoff law.

3. Results

3.1. Validity of Boyle-van't Hoff law

If liposomes or cells have the properties of ideal osmometers, their relative volume after equilibration in hypertonic solutions obeys Eq. 1 (Boyle-van't Hoff law). In this case, a plot of the reciprocal of the sample's optical absorbance (which is proportional to the ghost volume) versus the expected relative volume at equilibrium (V_{eq}/V_i) should yield a straight line [13]. Fig. 1, left panel shows results in which the absorbance of equilibrated ghost samples was measured as a function of sucrose concentrations between 0 and 200 mM. Fig. 1, right panel verifies the expected linear relationship between the reciprocal of the optical absorbance at 350 nm and V_{eq}/V_i.

3.2. Water permeation induced by various solutes

Fig. 2, upper panel shows the time course of experiments in which water permeation in ghosts was induced by membrane-impermeable solutes such as glucose, polyethylene glycol (average molecular weight: 400 g/mol), or sucrose. Due to differences in refractive index of the hypertonic solutions, the absorbance versus time traces obtained for the three solutes differ in their amplitudes, but their time-dependency is essentially identical. This is emphasized in Fig. 2, lower panel, where the absorbance changes are displayed on a normalized scale in which the three curves become virtually indistinguishable. This finding confirms that the observed process is indeed water permeation since it is unrelated to the nature of the osmotically active solute and depends only on the intrinsic water permeability of the ghost membranes. Since sucrose produced the largest amplitude change, it was used for the following water permeation experiments with α-hemolysin.

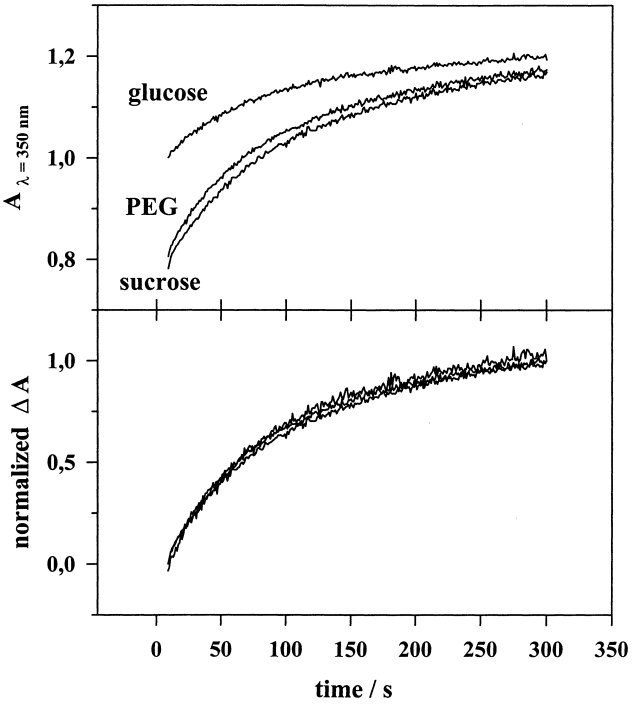

Fig. 2. Upper panel: Time course of absorbance (λ = 350 nm) of ghost samples (300 μl) diluted into 2 ml hypertonic solution (100 mM glucose, polyethylene glycol, or sucrose). Lower panel: Absorbance changes from the upper panel on a normalized scale on which the three curves coincide.

Because the optical absorbance was reciprocally proportional to the volume of the ghosts, the reciprocal of each absorbance versus time trace was fitted to a single-exponential decay. The resultant rate constant, k, was used to obtain the osmotic water permeability coefficient, P_f, according to the following equation [13,15,16]:

$$P_f = \frac{(1-V_{eq}/V_i)kV_i}{A\bar{V}_w\Delta c} = \frac{(1-c_i/(c_i+\Delta c))kr}{3\bar{V}_w\Delta c}. \quad (2)$$

Here, $\bar{V}_w$ was the molar volume of water and the term $(1-V_{eq}/V_i)$ specified the relative volume change of the ghosts required to reach osmotic equilibrium (see Eq. 1). The volume to surface ratio of the ghosts, V_i/A, was expressed as $r/3$, where r was taken to be a radius typical for rabbit red blood cells (3.35 μm; [17]). Δc was the difference in solute concentration between the inside and outside of the ghosts at the beginning of the experiment.

3.3. Water permeation as a function of toxin concentration and pH

The rate of water efflux from erythrocyte ghosts was markedly accelerated by the presence of α-hemolysin (Fig. 3). The increase in permeability attributed to the presence of α-hemolysin (ΔP) can be visualized easily when the permeability coefficient measured in the absence of toxin is subtracted from that measured in the presence of toxin. The results for ΔP measured at three channel to ghost ratios and three

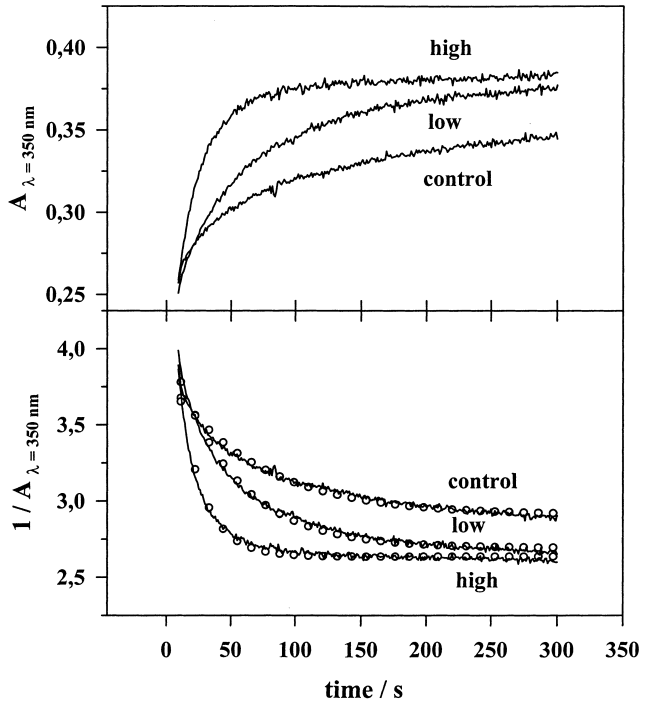

Fig. 3. The effect of α-hemolysin on water permeation in ghosts. Upper panel: Typical absorbance versus time traces at pH 7 for ghosts with ('low': 100 channels per ghost, 'high': 1000 channels per ghost) and without α-hemolysin channels ('control'). Hypertonic buffer: 100 mM sucrose in buffer B. Lower panel: Single-exponential fits (circles) to the reciprocals of the traces shown in the upper panel.

pH-values are summarized in Table 1. Fig. 4 illustrates that the increase in permeability is directly related to the amount of toxin present. Since hemolytic assays of the supernatant from the centrifugation step after the incubation period did not detect notable levels of hemolytic activity, it was assumed that most of the added α-hemolysin was associated with the ghosts (more than 94% in case of a nominal channel to ghost ratio of 200, for example). At all three pH-values, doubling the toxin concentration from 100 channels/ghost to 200 channels/ghost also doubled ΔP. Increasing the toxin concentration from 100 channels/ghost by a factor of 10 to 1000 channels/ghosts resulted in an increase in ΔP by a factor of 7 to 8.

To a lesser extent, the effect of α-hemolysin was also a function of pH. Comparing the bars in Fig. 4 shows that ΔP tended to become larger at lower pH-values. The increase in ΔP between pH 7 and pH 5 varied between 10% and 37%, depending on toxin concentration. Overall, the pH-induced changes were relatively small and only at high channel concentrations clearly exceeded the experimental error (Table 1).

It is noteworthy that even at high toxin concentrations, no noticeable sucrose influx into the ghosts occurred on the time scale of the experiments. If sucrose entered the ghosts, one would expect to see a biphasic pattern in which a decrease in absorbance follows the initial rise. This was clearly not the case here, although molecules of the size of sucrose should in principle fit through pores formed by α-hemolysin channels. Apparently, longer observation times and/or higher channel concentrations are required to observe noticeable sucrose permeation in this type of permeation experiment.

3.4. Water transport as a function of temperature

For the determination of the activation energy of water transport through α-hemolysin channels, the rate constants measured at temperatures between 10 and 40°C were used to construct an Arrhenius plot. Fig. 5 presents a semi-logarithmic plot in which the differences between the rate constants measured in the presence and absence of α-hemolysin are plotted against the reciprocal of temperature (pH 7, 200 channels/ghost). The slope of the plot in Fig. 5 was determined by linear regression and permitted the calculation of the activation energy, E_a (slope $= -E_a/R$).

Table 1
Channel-induced increase in the osmotic water permeability coefficient in ghosts at three channel concentrations and three pH-values

	pH 5	pH 6	pH 7
ΔP_{100}	$1.2 \pm 0.1 \times 10^{-4}$	$1.1 \pm 0.2 \times 10^{-4}$	$9.0 \pm 1.2 \times 10^{-5}$
ΔP_{200}	$2.1 \pm 0.2 \times 10^{-4}$	$2.2 \pm 0.1 \times 10^{-4}$	$1.9 \pm 0.1 \times 10^{-4}$
ΔP_{1000}	$9.3 \pm 0.5 \times 10^{-4}$	$7.9 \pm 0.1 \times 10^{-4}$	$6.8 \pm 0.2 \times 10^{-4}$
P_f	$1.5 \pm 0.2 \times 10^{-12}$	$1.5 \pm 0.2 \times 10^{-12}$	$1.3 \pm 0.2 \times 10^{-12}$

ΔP-values are permeability coefficients in cm/s measured in the presence of α-hemolysin after subtraction of the corresponding permeability coefficients for passive water permeation determined in the absence of α-hemolysin. Each entry represents the average and standard deviation of three repeats. The index specifies the channel to ghost ratio. The single-channel permeability coefficients, p_f, were calculated from ΔP_{100} and ΔP_{200} and are expressed in cm^3/s.

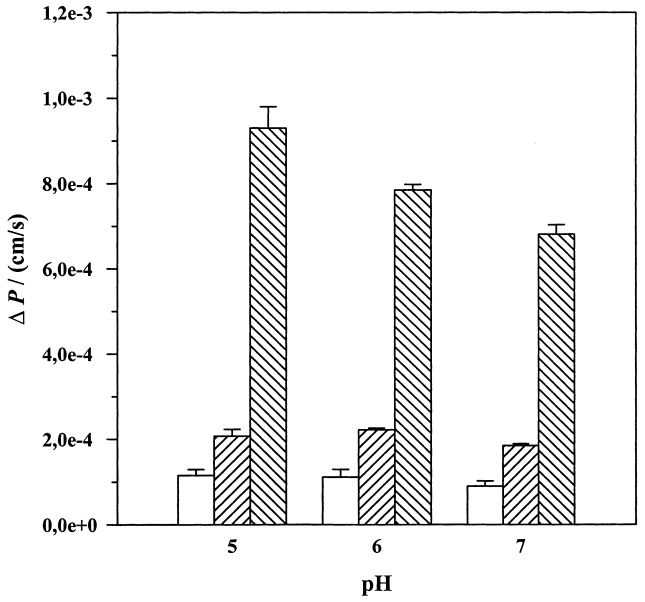

Fig. 4. Effect of pH and toxin concentration on the osmotic water permeability coefficient. ΔP is the permeability coefficient measured in the presence of toxin after subtraction of the passive water permeability coefficient. Left bars in each triplet: 100 channels per ghost, middle bars: 200 channels per ghost, right bars: 1000 channels per ghost. Each bar indicates the average of three repeats and the error bars represent the standard deviations.

4. Discussion

4.1. Single-channel permeability coefficients

The experimental data presented in the previous section clearly show that α-hemolysin increases the permeability of ghost membranes to water. A quantitative measure of the ability of channels to facilitate permeation of water or other solutes is commonly characterized by the single-channel conductance [18] or by the single-channel permeability coefficient [8,10,19,20]. Based on the measured values for ΔP, the osmotic single-channel permeability coefficient of α-hemolysin with respect to water can be calculated as follows:

$$p_f = \Delta P_f A/n. \quad (3)$$

For such an assessment it is necessary to know the ghost surface area (A) and the average number of channels present in a single erythrocyte ghost (n). If no red blood cells are lost during the preparation of the ghosts, the number of ghosts per volume equals the red blood cell count for rabbit blood which has been reported to be 6.3×10^{12} cells/l [21]. Assuming that all the α-hemolysin added to the ghosts formed channels, one expects an average number of 100, 200, and 1000 channels per ghost. These numbers are upper limits but should provide a valid estimate if the very high affinity of rabbit blood cells for the toxin is considered [1], particularly at low toxin concentrations. Incomplete channel insertion due to short incubation was avoided by exposing the ghosts to toxin for an extended period of time (1 h at 37°C plus 12 h at room temperature). Control experiments in which water permeation was measured immediately after the 37°C incubation period displayed the same kinetics as experiments in which the same sample had been kept at room temperature for an additional 2 h (data not shown). Presumably, most channels readily inserted during the 37°C incubation period which is consistent with other reports [1].

After the incubation step, the amount of toxin not associated with the ghosts was determined by centrifuging the samples and assaying the supernatant for hemolytic activity. Since the detected hemolytic ac-

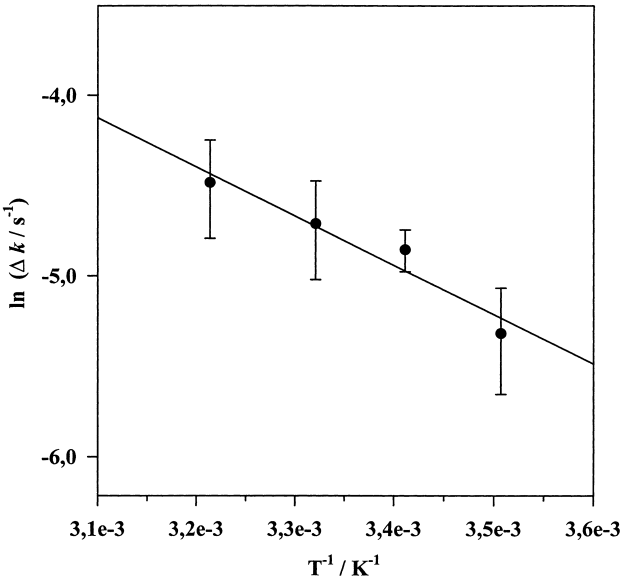

Fig. 5. Arrhenius plot for the assessment of the activation energy of water flow through α-hemolysin channels. Measurements were performed at pH 7 with a channel to ghost ratio of 200. Δk is the rate constant in the presence of channels minus the rate constant in the absence of channels. Each data point represents the average of three or four measurements and the bars indicate the standard deviations.

tivities were very low, it was concluded that most of the α-hemolysin was indeed bound by the ghosts. Finally, it should be noted that potential errors in the channel to cell ratio due to an overestimate of the number of incorporated channels will counteract or partially compensate errors due to cell loss during the ghost preparation.

As depicted in Fig. 4, the increase in permeability due to the presence of channels is related to the number of channels added. At all pH-values, doubling the channel concentration from 100 channels/ghost to 200 channels/ghost causes an increase in ΔP by a factor of two. Increasing the channel concentration by a factor of 10 from 100 to 1000 channels/ghost yields an increase in ΔP by a factor of 7 to 8, which is slightly lower than expected. A possible reason for this observation may be incomplete channel insertion at the higher toxin concentration, despite the prolonged incubation time. This explanation is consistent with the finding that channels bind exclusively to high-affinity sites located on the surface of rabbit erythrocytes at low toxin concentrations [1]. Once these receptor sites are saturated, binding of additional toxin occurs via absorptive interactions which are less efficient than the high-affinity sites. As a result, some of the toxin added at the higher concentration may bind to the membrane but not form functional channels. Since a high channel insertion efficiency is required for assessing single-channel permeability coefficients, only the ΔP-data obtained at the two lower toxin concentrations are included in the following discussion.

At pH 7, ΔP amounts to 9.0×10^{-5} cm/s and 1.9×10^{-4} cm/s for a channel to ghost ratio of 100 and 200, respectively. If the surface area of a ghost is approximated by that of a sphere with a radius typical for an erythrocyte (3.35 μm, [17]), one obtains a surface area of 1.4×10^{-6} cm^2, implying that the surface area per channel equals 1.4×10^{-8} cm^2 and 7.0×10^{-9} cm^2, respectively. According to Eq. 3, these values yield a single-channel permeability coefficient of 1.3×10^{-12} cm^3/s. If p_f is converted into the number of water molecules that pass through one channel in one second, one obtains 7.8×10^7 molecules under the experimental conditions specified above.

Typical examples for single-channel permeability coefficients reported in the literature for water are 9.6×10^{-15} cm^3/s for gramicidin A [19], 5.6×10^{-14} cm^3/s for certain water transporters found in toad bladders [10], 6×10^{-14} cm^3/s for the water channel CHIP 28 [20], 1.5×10^{-14} cm^3/s for double-length nystatin [22], 1×10^{-13} cm^3/s for single-length nystatin [22], and 4.5×10^{-14} cm^3/s for amphotericin B [22]. These numbers are up to two orders of magnitude smaller than the single-channel permeability coefficient estimated for α-hemolysin which is consistent with the much larger pore size of α-hemolysin.

4.2. Permeability coefficients and pore size

How does channel size correlate with the single-channel permeability coefficient? Water flow through aqueous channels can be quantified by applying hydrodynamic laws of laminar water flow, provided the dimensions of the pores are large enough to accommodate multiple water molecules with properties similar to those of bulk water. For channels of unknown size, the activation energy of water transport can serve as an indicator. The presence of large aqueous channels in membranes reduces the energy barrier from energies as high as 10 kcal/mol (a number typical for passive water permeation across unmodified bilayers) to values that are characteristic for water flow in the bulk phase (3–5 kcal/mol; [23,24]). The measured activation energy of 5.4 kcal/mol for water transport through α-hemolysin pores implies that the dimensions of the channel are large and that permeating water has bulk properties. Similar conclusions were reached by Belmonte et al. [6] who measured the activation energy for ion transport through α-hemolysin in planar bilayers.

In order to calculate single-channel permeability coefficients, Poiseuille's law can be used to correlate the number of water molecules that pass through a pore per second to pore length and radius [22,25]. The assumptions involved in this calculation are that the pore is static and has the shape of a cylinder. The single-channel permeability coefficient, p_f, for a cylindrical pore of radius r and length l is given by:

$$p_f = \frac{\pi R T r^4}{8\eta l \bar{V}_w}. \quad (4)$$

In the case of α-hemolysin, the choice of a particular value for r is somewhat arbitrary because the width of the pore formed by an α-hemolysin hep-

tamer is not uniform [3]. The narrowest gaps are found in the stem region of the channel which has a length of 52 Å and a radius varying between 7 and 12 Å. For this reason, two calculations will be carried out using a minimum pore radius of 7 Å and an averaged radius of 9.5 Å. The viscosity of water at room temperature, η, was taken as 10^{-3} kg/m/s.

Under these conditions, one obtains a single-channel permeability coefficient of 2.5×10^{-12} cm^3/s for a pore of radius 7 Å which is only slightly higher than the experimental average value of 1.3×10^{-12} cm^3/s at pH 7. If a radius of 9.5 Å is used, the calculated p_f is 8.5×10^{-12} cm^3/s which is considerably greater than the experimental result. As shown in Fig. 6 (dotted line), the extreme sensitivity of the calculated p_f to r makes it difficult to compute accurate single-channel permeability coefficients based on pore radii. Nevertheless, a rough estimate can be obtained and the results indicate that the smaller of the two radii matches the experimental result reasonably well.

Eq. 4 was developed for pores of macroscopic size in which the finite radius of water molecules (r_w) can be neglected. For smaller pores, a modified form of Eq. 4 has been introduced that contains correction terms accounting for steric restrictions of water molecules entering the pore and increased frictional interactions between water and pore walls [22,26,27]:

$$p_f = \frac{RT\pi r^4}{8\eta l \bar{V}_w}\left[2\left(1-\frac{r_w}{r}\right)^2-\left(1-\frac{r_w}{r}\right)^4\right]\left[1-2.104\left(\frac{r_w}{r}\right)+2.09\left(\frac{r_w}{r}\right)^3-0.95\left(\frac{r_w}{r}\right)^5\right]. \quad (5)$$

If p_f is calculated by Eq. 5 instead of Eq. 4 (Fig. 6, solid line), one predicts a single-channel permeability coefficient of 1.5×10^{-12} cm^3/s instead of 2.5×10^{-12} cm^3/s for a pore radius of 7 Å and of 5.9×10^{-12} cm^3/s instead of 8.5×10^{-12} cm^3/s for a pore radius of 9.5 Å, respectively (Fig. 6). As expected, these new numbers are slightly lower than those obtained from Eq. 4 and the p_f-value calculated for a radius of 7 Å compares favorably to the experimental results. Overall, these findings provide support for the concept that the physical properties of water inside the α-hemolysin channel are similar to those of bulk water since its flow is well characterized by macroscopic laws for laminar water flow.

Without any knowledge of the structure of α-hemolysin, one can get a rough estimate of the pore size by using experimentally determined water permeation rates and calculating a pore radius from the water permeation rate. When predicting r from p_f by Eq. 4 or 5, one benefits from the fact that even large uncertainties in the experimental value for p_f will cause only minor variations in r (Fig. 6). As a first approximation, a value of 50 Å will be assumed for the length of the channel, which is the minimum length required to span both the hydrophobic core and headgroup region of a typical biological membrane [28]. Knowing that p_f of the channel has a value of 1.3×10^{-12} cm^3/s, one calculates pore radii of 6.0 Å and 6.8 Å by using Eqs. 4 and 5, respectively. According to the X-ray structure, the latter radius matches the value for the narrow stem region but is somewhat lower than proposals based on single-channel conductance data (11.4 Å; [5]). Again, the calculated values should be considered a rough estimate since the following simplifications were involved in this calculation: the structure of the pore was assumed to be cylindrical, the length of the pore was somewhat underestimated, and gating properties of the channel were entirely neglected.

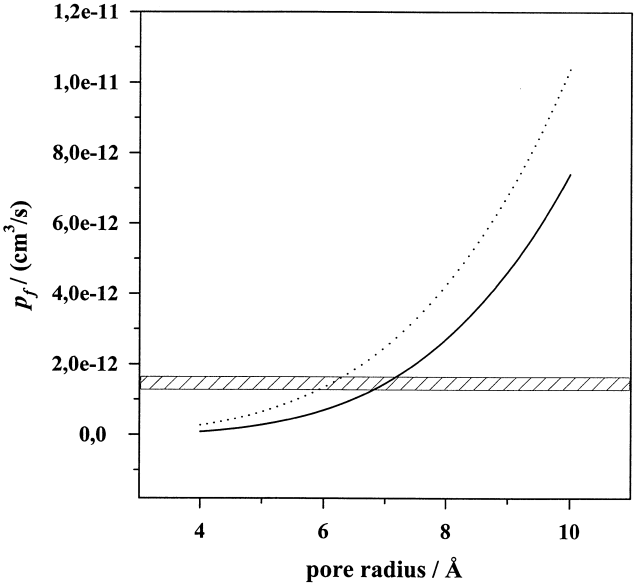

Fig. 6. The calculated single-channel water permeability coefficient (p_f) as a function of pore radius. The dotted line was obtained from Poiseuille's law (Eq. 4) and the solid line was calculated taking into account the molecular dimensions of water (Eq. 5). The grey area depicts the range of the experimentally determined single-channel permeability coefficients for α-hemolysin.

Although hydrodynamic calculations yield good agreement between observed and expected permeability coefficients, it is important to note that many channels are not simply static holes in membranes. Instead they undergo rapid changes between open and closed or partially closed conformations, which is commonly referred to as channel gating [18]. Single-channel permeability coefficients measured in the permeation experiments described above should therefore be regarded as average values which are obtained by sampling the average permeability of a large ensemble of channels in various configurations. Inspection of single-channel recordings shows that the lifetime of the open state in α-hemolysin is much greater than the lifetime of the closed state [7], implying that this particular channel remains open most of the time. It is therefore unlikely that gating leads to an underestimate of the single-channel permeability coefficient obtained from the water permeation experiments. For the same reason, the approximation of the channel structure by a *static* cylindrical pore in Eqs. 4 and 5 seems justified.

4.3. pH-effects

As revealed by Fig. 4, decreasing the pH from 7 to 5 causes a slight increase of the α-hemolysin-induced water permeability. The magnitude of this pH-effect depends to some extent on the amount of α-hemolysin and is most pronounced at high channel concentrations. There are several possible ways in which pH-changes can cause variations in the permeability coefficient of a channel. Perhaps the simplest explanation is a pH-dependent insertion efficiency of the channels into the ghost membranes. For example, it has been reported that lowering the pH from 8 to 4 leads to an enhanced permeability of small unilamellar vesicles by α-hemolysin from *Staphylococcus aureus* [29] and by hemolysin from *Escherichia coli* [30]. This observation was ascribed to a faster and more efficient insertion of channels into the bilayers rather than increased intrinsic channel permeability. It is unlikely that this effect is responsible for the experimental results reported here. First, the incubation of α-hemolysin with ghosts was carried out at pH 7 for all samples. After extended incubation that allowed ample time for maximum channel incorporation, the ghosts were washed twice, a procedure which would have removed any free channels in the supernatant. In case of samples used for measurements at low pH, this step was followed by a readjustment of the pH. Furthermore, control experiments demonstrated that the pH-effect was reversible (data not shown).

It is also known that changes in pH can affect the gating properties of channels. Kasianowicz and Bezrukov [7,31] noted such an effect when studying single-channel currents in α-hemolysin reconstituted in planar lipid bilayers. At pH 4.5, the frequency at which short-lived channel closures occurred was about 10 times higher than at pH 7.5. This effect would give rise to an overall decrease in the average single-channel permeability coefficient at lower pH-values and is therefore inconsistent with the detected increase.

Finally, pH-induced conformational changes can modify the geometric shape of the channel and thereby alter its effective pore size [32]. Similar effects can be caused by protonation of acidic residues lining the channel pore which influence the effective channel pore size for charged solutes by electrostatic interactions. Potential candidates for amino acids inside the channel with acid/base properties are histidine, glutamic acid, aspartic acid, or even lysine [7,33]. Kasianowicz and Bezrukov [7] found that single-channel currents of α-hemolysin reconstituted in planar bilayers increased by about 15% when the pH was changed from 7.5 to 4.5. Similar observations were made by Korchev et al. [34]. Given the substantial differences in experimental conditions of the planar bilayer studies and the water permeation experiments, this qualitative agreement of the results is remarkable. Overall, the most likely explanation for the pH-dependence of the α-hemolysin-induced water permeability in ghost membranes appears to be an increase in the effective pore size at lower pH.

Acknowledgements

This work was supported by NASA Grant NAG5-4665.

References

[1] S. Bhakdi, J. Tranum-Jensen, Alpha-toxin of *Staphylococcus aureus*, Microbiol. Rev. 55 (1991) 733–751.

[2] H. Bayley, Building doors into cells, Sci. Am. 277 (1997) 61–67.
[3] L. Song, M.R. Hobaugh, C. Shustak, S. Cheley, H. Bayley, J.E. Gouaux, Structure of staphylococcal α-hemolysin, a heptameric transmembrane pore, Science 274 (1996) 1859–1866.
[4] R. Füssle, S. Bhakdi, A. Sziegoleit, J. Tranum-Jensen, T. Kranz, H.-J. Wellensiek, On the mechanism of membrane damage by *Staphylococcus aureus* α-toxin, J. Cell Biol. 91 (1981) 83–94.
[5] G. Menestrina, Ionic channels formed by *Staphylococcus aureus* alpha-toxin: voltage-dependent inhibition by divalent and trivalent cations, J. Membr. Biol. 90 (1986) 177–190.
[6] G. Belmonte, L. Cescatti, B. Ferrari, T. Nicolussi, M. Ropele, G. Menestrina, Pore formation by *Staphylocoocus aureus* alpha-toxin in lipid bilayers. Dependence upon temperature and toxin concentration, Eur. Biophys. J. 14 (1987) 349–358.
[7] J. Kasianowicz, S. Bezrukov, Protonation dynamics of the α-toxin ion channel from spectral analysis of pH-dependent current fluctuations, Biophys. J. 69 (1995) 94–105.
[8] A. Finkelstein, The ubiquitous presence of channels with wide lumens and their gating by voltage, Ann. N. Y. Acad. Sci. 456 (1985) 26–32.
[9] R. Ye, A.S. Verkman, Simultaneous optical measurement of osmotic and diffusional water permeability in cells and liposomes, Biochemistry 28 (1989) 824–829.
[10] R. Zhang, A.S. Verkman, Water and urea permeability properties of *Xenopus* oocytes: expression of mRNA from toad urinary bladder, Am. J. Physiol. 280 (1991) C26–33.
[11] A. Bernheimer, Assay of hemolytic toxins, Methods Enzymol. 165 (1988) 213–217.
[12] T. Steck, J.A. Kant, Preparation of impermeable ghosts and inside-out vesicles from human erythrocyte membranes, Methods Enzymol. 31 (1974) 172–180.
[13] A.D. Bangham, J. De Gier, G.D. Greville, Osmotic properties and water permeability of phospholipid liquid crystals, Chem. Phys. Lipids 1 (1967) 225–246.
[14] T. Terwilliger, A.K. Solomon, Osmotic water permeability of human red cells, J. Gen. Physiol. 77 (1981) 549–570.
[15] J. De Gier, Osmotic behaviour and permeability properties of liposomes, Chem. Phys. Lipids 64 (1993) 187–196.
[16] M. Jansen, A. Blume, A comparative study of diffusive and osmotic water permeation across bilayers composed of phospholipids with different head groups and fatty acyl chains, Biophys. J. 68 (1995) 997–1008.
[17] T.A.J. Prankerd, The Red Cell, Blackwell Scientific Publications Ltd., Oxford, 1961.
[18] B. Hille, Ionic Channels of Excitable Membranes, Sinauer Associates Inc., Sunderland, 1984.
[19] P.A. Rosenberg, A. Finkelstein, Interaction of water and ions in gramicidin A channels. Streaming potentials across lipid bilayer membranes, J. Gen. Physiol. 72 (1978) 327–340.
[20] A.N. Van Hoek, M. Wiener, S. Bicknese, L. Miercke, J. Biwersi, A.S. Verkman, Secondary structure analysis of purified functional CHIP28 water channels by CD and FTIR spectroscopy, Biochemistry 32 (1993) 11847–11856.
[21] R. Parmley, in: A.F. Rowley, N.A. Ratcliffe (Eds.), Vertebrate Blood Cells, Cambridge University Press, Cambridge, 1988, pp. 337–424.
[22] A. Finkelstein, Water Movement through Lipid Bilayers, Pores, and Plasma Membranes: Theory and Reality, Wiley Interscience, New York, 1987.
[23] A.S. Verkman, J.A. Dix, J.L. Seifter, Water and urea transport in renal microvillus membrane vesicles, Am. J. Physiol. 248 (1985) F650–655.
[24] M.A. Suleymanian, C.M. Baumgarten, Osmotic gradient-induced water permeation across the sarcolemma of rabbit ventricular myocytes, J. Gen. Physiol. 107 (1996) 503–514.
[25] C.R. Cantor, P.R. Schimmel, Biophysical Chemistry, Freeman and Company, New York, 1980, pp. 643–645.
[26] E.M. Renkin, Filtration, diffusion, and molecular sieving through porous cellulose membranes, J. Gen. Physiol. 38 (1954) 225–243.
[27] C.V. Paganelli, A.K. Solomon, The rate of exchange of tritiated water across the human red cell membrane, J. Gen. Physiol. 41 (1957) 259–277.
[28] M.C. Wiener, S.H. White, Structure of a fluid dioleoylphosphatidyl-choline bilayer determined by joint refinement of x-ray and neutron diffraction data. III. Complete structure, Biophys. J. 61 (1992) 437–447.
[29] S. Forti, G. Menestrina, Staphylococcal α-toxin increases the permeability of lipid vesicles cholesterol- and pH-dependent assembly of oligomeric channels, J. Biochem. 181 (1989) 767–773.
[30] G. Menestrina, *Escherichia coli* hemolysin permeabilizes small unilamellar vesicles loaded with calcein by a single-hit mechanism, FEBS Lett. 232 (1988) 217–220.
[31] S. Bezrukov, J. Kasianowicz, The charge state of an ion channel controls neutral polymer entry into its pore, Eur. Biophys. J. 26 (1997) 471–476.
[32] D.H. Hoch, A. Finkelstein, Gating of large toxin channels by pH, Ann. N. Y. Acad. Sci. 456 (1985) 33–35.
[33] L. Cescatti, C. Pederzolli, G. Menestrina, Modification of lysine residues of *Staphylococcus aureus* α-toxin: effects on its channel forming properties, J. Membr. Biol. 119 (1991) 53–54.
[34] Y.E. Korchev, G.M. Alder, A. Bakhramov, C.L. Bashford, B.S. Joomun, E.V. Sviderskaya, P.N.R. Usherwood, C.A. Pasternak, *Staphylococcus aureus* alpha-toxin-induced pores: channel-like behavior in lipid bilayers and patch clamped cells, J. Membr. Biol. 143 (1995) 143–151.